Contents lists available at ScienceDirect

Computers & Graphics

journal homepage: www.elsevier.com/locate/cag

MIA: A Visual Analytics System for Multimodal Spectral Imaging Data

Hennes Rave[a,*], Katharina Kronenberg[a,b], Hannes Gödde[a], Lea Tobergte[a], Michael Holtkamp[a], Julia Werner[c], Peter Bohrer[c], Fabian Lohöfer[c], Rickmer Braren[d], David Clases[b], Uwe Karst[a], Lars Linsen[a]

[a] *University of Münster, Germany*
[b] *University of Graz, Austria*
[c] *Technical University of Munich, Germany*
[d] *University Medical Center Hamburg-Eppendorf, Germany*

arXiv:2606.00874v1 [cs.HC] 30 May 2026

ARTICLE INFO

Article history:
Received June 2, 2026

Keywords: Hyperspectral Imaging, Visual Analytics, Dimensionality Reduction, Interactive Segmentation, Multimodal Analysis, Bioimaging

ABSTRACT

Hyperspectral bioimaging techniques such as infrared (IR) microscopy and laser ablation-inductively coupled plasma-mass spectrometry (LA-ICP-MS) produce high-dimensional, spatially resolved datasets that require sophisticated analysis to reveal chemically and anatomically meaningful structures. Existing software solutions are typically modality-specific and cover only parts of the analytical workflow, forcing researchers to transfer data across multiple tools and manually reconcile results. We present MIA (Multiscale Image Analysis), a modality-agnostic visual analysis environment that integrates the full exploratory workflow – from spectral preprocessing and dimensionality reduction to interactive segmentation and spectral similarity analysis – within a single, tightly coupled interface. MIA supports hierarchical and landmark-based embeddings to handle datasets of varying scale and complexity, interactive and automatic segmentation with a shared state across all linked views, and multimodal analysis of co-registered datasets from different instruments. We demonstrate the effectiveness of MIA through three use cases drawn from real analytical chemistry workflows: (1) the recovery of biologically meaningful tissue compartments through derivative preprocessing and hierarchical embedding, (2) pigment identification via spectral similarity search with spatial overview, and (3) multimodal tissue characterization combining molecular IR and elemental LA-ICP-MS data. Qualitative feedback from domain expert collaborators confirms that MIA reduces the need for tool-switching and supports analytical insights that are difficult to obtain with existing software.

© 2026 Elsevier B.V. All rights reserved.

1. Introduction

Hyperspectral bioimaging has become an increasingly important tool across the biomedical and analytical sciences. Techniques such as quantum cascade laser (QCL)-based infrared (IR) microscopy, micro x-ray fluorescence (micro-XRF), and laser ablation-inductively coupled plasma-mass spectrometry (LA-ICP-MS) acquire spatially resolved measurements with up to thousands of spectral channels, producing high-dimensional datasets that encode rich molecular and elemental information about biological tissue, materials, and environmental samples [1, 2, 3, 4]. The growing availability of these instruments and the emergence of workflows that combine multiple hyperspectral modalities on the same specimen have created a pressing need for flexible, interactive software that can support the full analytical pipeline.

Extracting meaningful information from hyperspectral bioimaging data is inherently a multi-step process. Raw spec-

*Corresponding author: hennes.rave@uni-muenster.de

tra typically require preprocessing such as baseline correction, normalization, or the computation of spectral derivatives before structure becomes apparent. Dimensionality reduction is then used to embed the high-dimensional spectra into a low-dimensional space where spectrally similar pixels cluster together, providing a basis for segmentation. Segmentation itself is rarely fully automatic: domain experts routinely refine automatic clusterings by inspecting individual segments in both spatial and spectral terms, merging or splitting regions based on domain knowledge. Finally, the resulting segments are interpreted through spectral exploration, comparing per-segment summary spectra, computing similarities to reference spectra, or examining the distribution of individual channels across segments. Crucially, these steps are not sequential but iterative: a segmentation may prompt re-examination of the embedding, which may in turn motivate a different preprocessing strategy. Manual segmentation by domain experts is, however, inherently subjective, with variability between observers depending on training and institutional conventions [5]. Reproducible algorithmic approaches that integrate expert refinement with transparent automatic clustering can mitigate this variability.

Existing software solutions address parts of this workflow, but rarely the whole. Tools designed for IR spectroscopy, such as Quasar [6, 7], provide strong preprocessing pipelines but follow a node-based workflow paradigm that limits interactive exploration and lacks support for hierarchical or scalable embedding methods. Tools targeting LA-ICP-MS focus primarily on elemental map generation and quantitative analysis, with limited support for embedding-based exploration or interactive segmentation across linked views. Broader mass spectrometry imaging platforms such as Cardinal [8, 9] and commercial tools such as SCiLS Lab provide statistical analysis capabilities but are typically instrument-specific and restrict cross-modality workflows to vendor-specific datasets. As a result, researchers routinely transfer data between multiple disconnected tools, a process that is time-consuming, error-prone, and difficult to reproduce.

We present *MIA* (Multiscale Image Analysis), a modality-agnostic visual analysis environment designed to support the full exploratory workflow for hyperspectral bioimaging data within a single, tightly coupled interface. MIA treats any dataset as a collection of pixels with associated spectra and spatial coordinates, enabling it to handle any spectral imaging modality such as IR microscopy, LA-ICP-MS, micro-XRF, and multimodal combinations thereof without modification. A shared segmentation state propagates across all linked views, ensuring that every interaction, whether a lasso selection in the embedding, a manual edit in the image viewer, or an automatic clustering, is immediately reflected throughout the interface. To handle the scale and complexity of real-world datasets, MIA supports landmark-based UMAP [10] for datasets of millions of pixels, as well as hierarchical embeddings that allow users to iteratively refine the analysis within individual segments. MIA is open source and freely available at `https://github.com/hennesrave/multiscale-image-analysis`.

The contributions of this paper are:

- A modality-agnostic visual analysis environment for (multimodal) hyperspectral bioimaging that integrates spectral preprocessing, embedding-based dimensionality reduction, interactive segmentation, and spectral exploration within a single linked-view interface with a shared segmentation state.
- An interactive hierarchical embedding workflow that combines spectral derivative preprocessing with successive UMAP refinements, enabling the iterative resolution of tissue structure at multiple scales within a single session.
- A validation of MIA through three real-world analytical chemistry workflows, demonstrating that the integrated design reduces tool-switching, supports emergent analytical strategies beyond those explicitly designed for, and enables insights that neither individual modalities nor manual approaches can reliably produce.

In the following, we first review related work on hyperspectral imaging software and embedding-based analysis methods in Section 2. We, then, present the MIA system, its data model, its visual encodings, and interaction mechanisms in Section 3. We apply MIA within three use cases drawn from real analytical chemistry workflows in Section 4 and discuss expert feedback, limitations, and directions for future work in Section 5.

2. Related Work

2.1. IR Spectroscopy Imaging Software

Infrared microscopy produces spatially resolved hyperspectral data that requires dedicated preprocessing before meaningful analysis is possible. The most widely used open-source tool for this domain is Quasar [6, 7], a distribution of the Orange data-mining platform [11] extended with spectroscopy-specific components. Quasar supports a broad range of preprocessing operations and integrates machine learning methods such as PCA [12], clustering, and classification into a visual workflow-builder paradigm, in which components are connected as nodes in a pipeline. While this approach is flexible and accessible, it differs fundamentally from MIA's design: Quasar does not provide linked spatial and spectral views that share a common segmentation state, does not support hierarchical or landmark-based UMAP for interactive exploration of large datasets, and is not designed for multimodal analysis across different instrument types. Commercial tools such as Cytospec [13] and Bruker OPUS [14] offer IR-specific preprocessing and visualization but are hardware-tied and offer limited support for modern dimensionality reduction or interactive segmentation.

2.2. LA-ICP-MS Software

LA-ICP-MS bioimaging software has historically focused on data reduction and elemental map generation. Open-source tools such as LA-iMageS [15] provide automated processing and visualization of elemental distribution images, while commercial platforms such as iolite from Elemental Scientific Lasers [16] and HDIP from Teledyne Photon Machines [17] offer comprehensive data reduction pipelines, automated workflows, and integrated 2D and 3D visualization of elemental

maps. HDIP additionally includes feature recognition and automated image processing tools. Several other tools targeting LA-ICP-MS data exist, including Pew^2 [18], an open-source image processing package compatible with common ICP-MS vendors, MeXpose [19], which provides quantitative single-cell metal bioaccumulation analysis, and TOFHunter [20], which enables rapid untargeted screening of ICP-TOF-MS data. While these platforms differ in focus and feature set, none provide an integrated workflow that combines embedding-based dimensionality reduction, interactive segmentation across linked spatial and spectral views, and modality-agnostic multimodal analysis as in MIA. The growing application of UMAP-based analysis to LA-ICP-TOFMS datasets [21, 22] highlights the scientific need for embedding-based exploration of this data type.

2.3. Molecular Mass Spectrometry Imaging Software

Molecular mass spectrometry imaging (MSI) is a related field that has attracted more software development effort, providing useful context for MIA's positioning. Cardinal [8, 9] is an R-based open-source package offering comprehensive statistical analysis of MSI data, including preprocessing, spatial segmentation, and classification. While analytically powerful, Cardinal operates primarily as a scripting environment and provides limited support for interactive visual exploration. The commercial SCiLS Lab platform offers a more interactive interface but is instrument-specific. M2aia [23] is an open-source application providing interactive visualization and 3D reconstruction for multimodal MSI datasets, and is the closest existing tool to MIA in terms of interactivity and multimodal support. However, M2aia is designed specifically for molecular MS modalities and does not support IR microscopy or LA-ICP-MS data. More broadly, as noted in recent work, most MSI tools target specific steps in the analytical pipeline or specific instrument families, leaving researchers to integrate multiple tools for a complete workflow. MIA addresses this gap across the IR, LA-ICP-MS, and micro-XRF domains by providing a unified, modality-agnostic environment that spans the full workflow from preprocessing to spectral exploration.

2.4. Dimensionality Reduction and Embedding in Bioimaging

Dimensionality reduction has become a central component of exploratory analysis for high-dimensional bioimaging data. Uniform Manifold Approximation and Projection (UMAP) [10] has emerged as the method of choice for this task due to its ability to preserve both local and global structure at superior runtime compared to t-SNE [24], making it particularly suited to the large datasets produced by modern imaging instruments. A recent survey on the application of dimensionality reduction in different application domains, including biology and chemistry, confirms this observation [25]. UMAP has been applied extensively in single-cell transcriptomics and, more recently, in spatial bioimaging contexts [2, 21], where it enables the identification of spatially coherent tissue regions that are not apparent in individual channel images. For very large datasets, landmark-based UMAP approximations reduce computational cost by computing the embedding on a representative subset of points and projecting the remaining data, making interactive exploration of datasets with millions of pixels feasible. For spatially or spectrally complex data, hierarchical approaches that iteratively re-embed subsets of the data allow users to refine the analysis within individual clusters, revealing fine-grained structure that global embeddings may obscure [26, 27, 21]. Graph-based clustering methods such as the Leiden algorithm [28] complement UMAP by operating directly on the nearest-neighbor graph used to construct the embedding, often producing more stable and well-connected clusters than K-means or density-based alternatives [29]. MIA integrates all of these methods – standard, landmark, and hierarchical UMAP, combined with Leiden, HDBSCAN [30], and K-means clustering – into a single interactive environment, directly connecting the embedding to spatial and spectral views through a shared segmentation state.

2.5. Visual Analysis of Hyperspectral Imaging Data

From the visualization community, Gerbil [31] is one of the most closely related general-purpose frameworks for interactive hyperspectral image analysis. It combines linked spectral and spatial views, interactive segmentation, and nonlinear false-color coding within a unified interface and has been applied to remote sensing and cultural heritage data. When compared to MIA, Gerbil is designed for reflectance spectroscopy rather than bioimaging modalities, does not support embedding-based dimensionality reduction or multimodal datasets, and targets a different user community. Jawad et al. [32] propose an interactive visual analysis approach for molecular MSI data using linear and non-linear embeddings in coordinated image-space and spectral-space views, demonstrating that embedding-driven cluster selection can faithfully recover ground-truth image regions. Their approach is conceptually close to MIA's embedding-segmentation workflow, but targets molecular MSI specifically and does not support hierarchical or landmark-based embeddings, multimodal datasets, or interactive spectral similarity analysis. Further visualization-community contributions have addressed related subproblems. Zhu et al. [33] use a cascade neural network to generate user-guided scatterplot embeddings for interactive hyperspectral image classification, with reuse of the trained network across time-varying datasets. Yu and Li [34] propose a feature-selection-oriented interactive visual analysis approach that guides the selection of spectral bands through information-theoretic indicators. Both target remote sensing applications rather than bioimaging. At the opposite end of the modality spectrum, Cell2Cell by Mörth et al. [35] presents a visual analytics system for analyzing cell-cell interactions in 3D multi-channel tissue data, combining graph-based interaction analysis with cell-centered polarization views. While the multi-channel imaging context is related, Cell2Cell operates on volumetric protein-expression data with only a handful of channels, rather than on hyperspectral data with hundreds or thousands of channels per pixel.

3. MIA: System Overview

MIA is a desktop application for the interactive visual analysis of hyperspectral bioimaging data. Figure 1 shows the

main application window, which consists of five coordinated views: the Spectrum Viewer (a), Image Viewer (b), Embedding Viewer and Channel Glyph Viewer (c, shared via tabs), and Histogram/Boxplot Viewers (d, e). The views are linked through a shared segmentation state: any change to the segmentation, whether through manual lasso selection, automatic clustering, or segment merging, is immediately reflected in all views simultaneously. Most functionality is accessible through context menus, keeping the interface uncluttered while supporting a wide range of operations. MIA is modality-agnostic: it operates on a common data model that accommodates IR microscopy, LA-ICP-MS, micro-XRF, and other hyperspectral imaging modalities without modification. MIA is implemented in C++ and is openly available at `https://github.com/hennesrave/multiscale-image-analysis`.

3.1. Data Model and Terminology

MIA operates on a *dataset* consisting of *pixels*, i.e., individual measurement points, each associated with a *spectrum* (one intensity value per channel) and a pair of spatial coordinates. The dataset is organized as a matrix of N pixels by C channels, where C ranges from tens of channels for modalities such as LA-ICP-MS to several thousand for micro-XRF.

A *segmentation* partitions the set of pixels into disjoint *segments*, each with an assigned name and color. A segment may consist of multiple disjoint regions in the image, reflecting the fact that pixels are typically assigned to segments based on spectral similarity rather than spatial proximity. The segmentation is global: it is shared across all views and all modalities in a multimodal session, ensuring consistency throughout the analysis. Pixels not yet assigned to any segment are treated as belonging to an implicit background.

A *feature* maps each pixel to a single scalar value and is used as the basis for image display, histograms, and boxplots. Features can be defined by selecting a single channel, integrating a range of channels with optional baseline correction, or combining existing features through arithmetic operations.

An *embedding* maps pixels – or, in the channel embedding, channels – to 2D points such that similar items are positioned close together. Embeddings are computed on demand and stored for reuse. They do not modify the underlying dataset.

3.2. Spectrum Viewer

The Spectrum Viewer displays the dataset's channels on the horizontal axis and intensity on the vertical axis. For each segment, it shows a configurable summary spectrum (minimum, maximum, or average) over all pixels belonging to that segment, color-coded by segment color. The global summary over all pixels is shown in black as a reference.

Users interact with the Spectrum Viewer primarily to create features and to preprocess the dataset. Clicking or dragging over the spectral axis creates a new feature by selecting a single channel or integrating a range; integration supports multiple accumulation modes and baseline correction options (from zero, from the local minimum, or from a linear baseline connecting the range endpoints). Dataset-wide preprocessing operations include baseline correction and the computation of spectral derivatives up to the third order, which are applied in-place and can substantially improve cluster separation in the embedding, as demonstrated in Section 4.1.

The Spectrum Viewer also supports spectral similarity analysis: users can import one or more reference spectra and compute a pixelwise similarity image using either Euclidean distance or cosine similarity. The resulting similarity values are exported as a new dataset, enabling downstream spatial analysis. Reference spectra can additionally be exported for use in other tools or shared across sessions.

3.3. Image Viewer

The Image Viewer provides spatial context by rendering pixels at their measured x/y coordinates, mapping the values of a selected feature to colors via a configurable colormap. A segmentation overlay or false-coloring can be displayed at adjustable opacity, allowing the feature image and the segmentation to be inspected simultaneously using α-blending.

The segmentation can be modified interactively in the Image Viewer using lasso selections. Automatic segmentations can be created using K-means, HDBSCAN [30], or the Leiden algorithm [28], applied either to the raw dataset or to a previously computed embedding. Segments can be added, removed, renamed, merged, and recolored through the context menu, and segmentations can be imported and exported for reproducibility.

False-coloring assigns colors to pixels based on their position in a 2D embedding rather than on segment membership, providing a continuous coloring that reveals fine-grained spatial structure even within segments. To increase contrast, MIA applies a density-equalizing transformation [36] to the embedding coordinates before mapping them into polar coordinates and into the $C = 35$ disk of the CIELCh color space, increasing inter-point distances in dense regions while preserving neighborhood structure, see Figure 2.

3.4. Embedding Viewer

The Embedding Viewer displays a 2D embedding of a selected set of channels or features for a chosen subset of pixels, with each point representing one pixel. Points are colored by segment membership or by false-coloring, and the view is linked to the Image Viewer such that lasso selections in the embedding space are immediately reflected as spatial selections in the image.

Embeddings are computed using UMAP [10], PCA [12], or t-SNE [24], with user control over which pixels, channels, and features are included, the normalization strategy (z-score, min-max, or none), and whether to export the underlying model for projection of new data.

For large datasets, MIA supports *landmark-based UMAP* [10], which computes the embedding on a representative subset of pixels and projects the remaining data onto the learned manifold. This makes interactive exploration of datasets with millions of pixels feasible without requiring specialized hardware.

Hierarchical embeddings allow users to iteratively refine the analysis by re-embedding only the pixels belonging to one or more selected segments. This is particularly useful when a

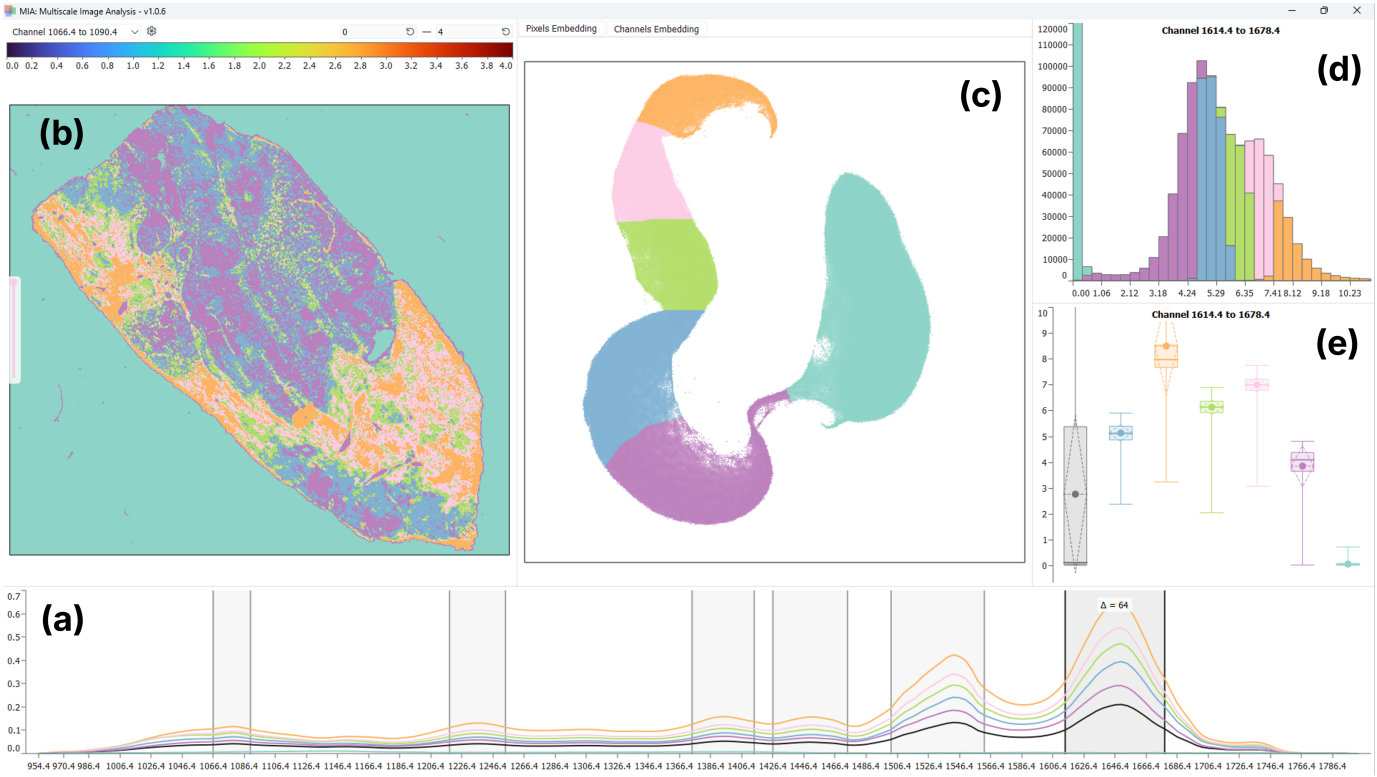

Fig. 1. The MIA application window showing all five views on an IR microscopy dataset of a tumor-bearing rat liver [2]. (a) Spectrum Viewer displaying per-segment average spectra and the global average in black; (b) Image Viewer showing the segmentation overlay; (c) Embedding Viewer (and Channel Glyph Viewer, accessible via tabs), showing a UMAP embedding with points color-coded by segment; (d) Histogram Viewer showing the frequency distribution and (e) Boxplot Viewer showing the intensity distribution for a selected feature.

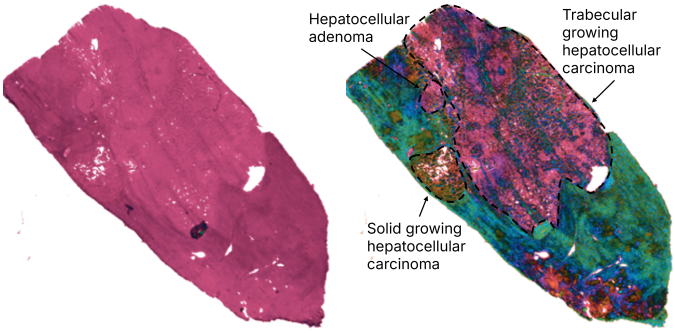

Fig. 2. False-coloring of a 213-channel IR microscopy image of a tumor-bearing rat liver [2], derived from a PCA embedding of the pixel spectra. Without contrast enhancement (left), dense regions of the embedding compress into similar colors. With the density-equalizing transformation applied (right), tissue substructures (indicated by manual annotations) become more visible.

global embedding reveals broad macro-structure but obscures finer distinctions within individual clusters; re-embedding a subcluster at higher effective resolution can reveal meaningful sub-populations, as demonstrated in Section 4.1. Pixels not yet assigned to a segment can be assigned to their nearest neighbor in the embedding space, supporting a semi-automatic segmentation workflow.

3.5. Channel Glyph Viewer

The Channel Glyph Viewer provides a glyph-based overview of the entire dataset at the level of channels rather than pixels. Each channel is represented as a small spectral glyph with a customizable color map, and the layout of the glyphs can be configured in three modes, see Figure 3. In *linear* mode, glyphs are arranged row by row in channel order, providing a compact overview of all channels simultaneously. In *embedding* mode, glyph positions are determined by a UMAP embedding of the channels, computed from a selected similarity metric (Pearson correlation, mutual information, Euclidean, or cosine), grouping similar channels together. In *gridified* mode, overlaps between glyphs are resolved by assigning them to discrete grid positions using Linear Sum Assignment [37], preserving the neighborhood structure of the embedding while ensuring legibility.

Per-segment channel abundances, computed by accumulating intensities per channel per segment, can be overlaid as donut charts, providing a concise summary of how intensity is distributed across segments for every channel simultaneously (see supplementary video).

In practice, users have also employed the Channel Glyph Viewer in linear mode as a spatial overview of similarity images computed in the Spectrum Viewer, treating each channel as one similarity map. This emergent use was not part of the original design intent, and is discussed further in Section 4.2.

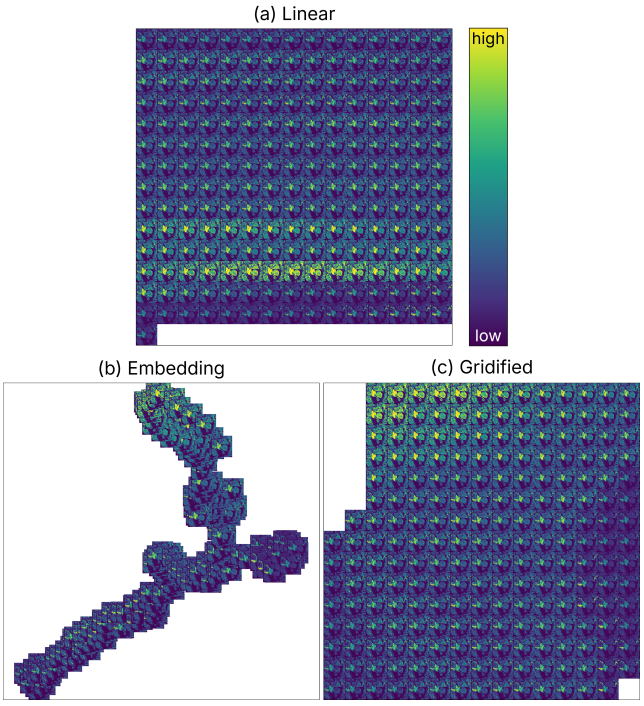

Fig. 3. The three layout modes of the Channel Glyph Viewer, shown on a QCL-IR microscopy dataset with 211 spectral channels. (a) *Linear* mode arranges glyphs row by row in channel order. (b) *Embedding* mode positions glyphs according to a UMAP embedding of the channels, grouping spectrally similar channels together at the cost of overlapping glyphs. (c) *Gridified* mode resolves these overlaps by assigning glyphs to discrete grid positions via Linear Sum Assignment, preserving the embedding's neighborhood structure while ensuring full glyph legibility.

3.6. Histogram and Boxplot Viewers

The Histogram Viewer displays the distribution of intensities for a selected feature as a stacked histogram, with each segment contributing a separate colored layer. The Boxplot Viewer shows the same information as individual boxplots for each segment alongside a boxplot for the dataset as a whole, supporting rapid visual comparison of per-segment intensity ranges and outlier structure. Both viewers respond to changes in the active segmentation and feature selection. These views are used less frequently than the embedding and image views in typical workflows, but provide complementary distributional information per segment.

3.7. Multimodal Analysis

MIA supports the simultaneous analysis of multiple co-registered datasets from different modalities. Having loaded a dataset, an additional dataset is imported via the Spectrum Viewer and, if the two datasets differ in spatial resolution, a registration dialog allows the user to manually align them. The imported dataset is then resampled to match the spatial resolution of the primary dataset using a user-selected interpolation scheme (nearest neighbor or bilinear). Each imported dataset is opened in a separate application window containing the full set of coordinated views, allowing each modality to be analyzed individually. The segmentation is shared across all windows, ensuring that every segment is defined consistently, regardless of how many co-registered modalities are loaded.

Multimodal embeddings are created in the Embedding Viewer by selecting channels or features from multiple datasets simultaneously. When more than one modality is selected, a weighting dialog allows the user to control the relative contribution of each modality to the final embedding. This is important in practice because modalities can differ substantially in channel count, and naive concatenation would cause the high-channel-count modality to dominate the embedding geometry.

4. Use Cases

The following use cases are drawn from real analytical workflows developed in close collaboration with domain experts in analytical chemistry. In each case, the dataset and workflow were provided by a collaborating researcher. We reproduce the analysis steps within MIA and report the results. The use cases are ordered from the most common workflow pattern to more specialized applications, reflecting the range of scenarios encountered in practice.

4.1. Use Case 1: Tissue Segmentation via Hierarchical Embedding

Dataset and goal. The first use case is based on a QCL-IR microscopy dataset of a tissue cross-section of a chicken embryo torso. The dataset consists of 9 000 000 pixels at a spatial resolution of 3000×3000 and 211 spectral channels covering the mid-infrared fingerprint region from 950 to 1800 cm^{-1}. The analytical goal is to segment the tissue into biologically meaningful regions, in particular, to separate distinct tissue types that differ in chemical composition, and to characterize their spectral signatures.

Step 1: Embedding of raw spectra. As a first step, a UMAP embedding is computed on the raw spectra using all 211 channels. Figure 4a shows the resulting embedding alongside the corresponding image view. Besides one small detached cluster corresponding to the gall bladder, the embedding reveals only a broad, poorly separated structure: a single dominant group of points with two minor protrusions, which are difficult to delineate cleanly into interpretable tissue regions. This result is typical for raw IR spectra, where baseline variation and broad, overlapping absorption bands dominate the inter-pixel distances and obscure the underlying chemical differences.

Step 2: Spectral derivative preprocessing. To suppress baseline effects and enhance the discriminability of spectral features, the second derivative is computed along the spectral dimension across the entire dataset using the Spectrum Viewer. The second derivative attenuates broad baseline contributions and resolves shoulder bands within overlapping absorption features, effectively acting as a high-pass filter in the spectral domain. A new UMAP embedding is then computed on the derivative spectra. As shown in Figure 4b, the resulting embedding exhibits substantially clearer cluster structure: the previously amorphous group of points resolves into several distinct clusters corresponding to the heart, bone, and a larger cluster

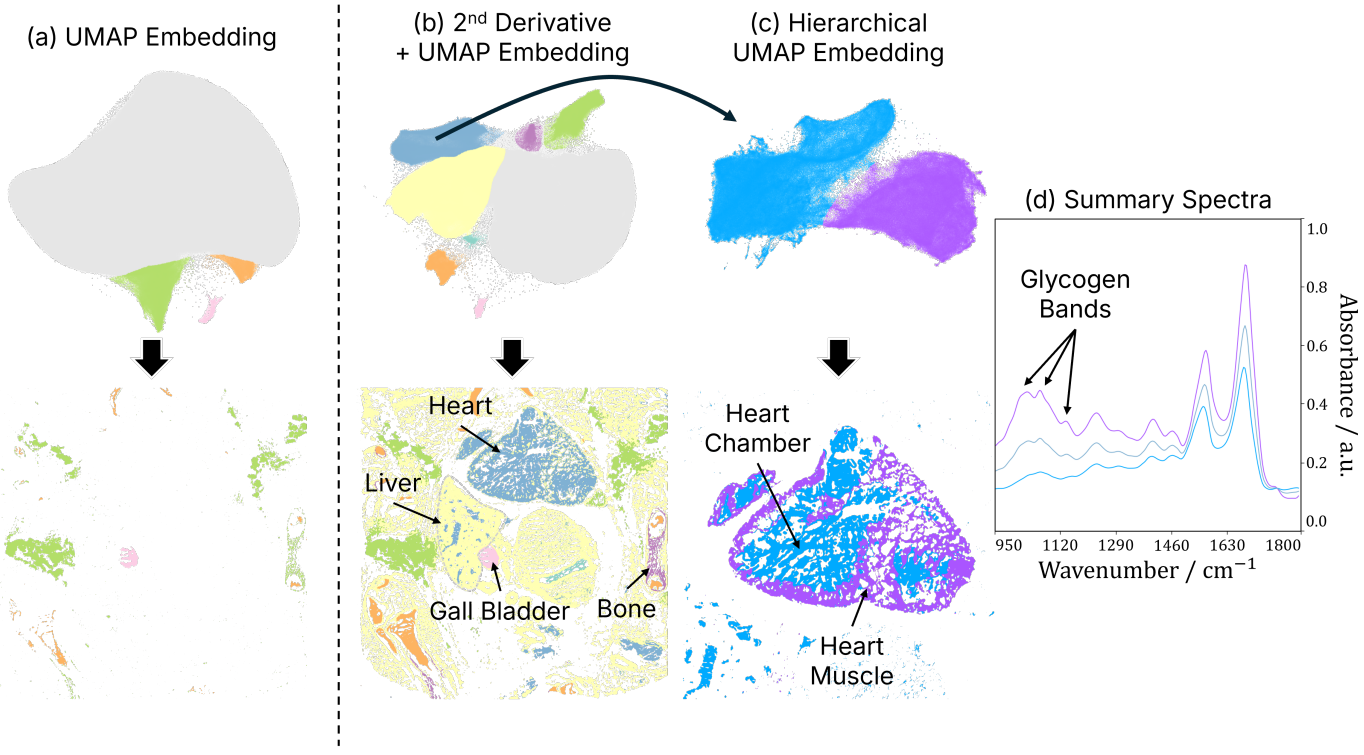

Fig. 4. Use Case 1: Tissue segmentation via hierarchical embedding on a QCL-IR microscopy dataset of a chicken embryo (tissue cross-section of the torso). (a) UMAP embedding (top) and image view (bottom) computed on raw spectra: no meaningful cluster structure is apparent. (b) After computing the second derivative along the spectral dimension, the UMAP embedding reveals clear cluster structure corresponding to spatially coherent tissue regions. (c) Hierarchical UMAP computed on a single subcluster separates the heart chamber from the heart muscle. (d) Spectrum Viewer showing the average spectra of the two subclusters compared to the average spectrum of the parent cluster before hierarchical refinement: the subclusters are chemically distinct, while the parent spectrum is a blurred average of both signatures, confirming that the hierarchical embedding successfully resolves two tissue types that the global embedding grouped together.

encompassing the liver and surrounding tissue, while the gall bladder remains a well-defined, isolated cluster as before.

Step 3: Hierarchical embedding for subcluster refinement. While the second-derivative embedding provides a useful initial segmentation, the heart cluster contains pixels from two spatially distinct regions that are not resolved at the global embedding scale. To refine the analysis, a hierarchical embedding is computed: only the pixels belonging to this cluster are selected, and a new UMAP embedding is computed on this subset. This increases the effective resolution of the embedding within the subcluster, allowing finer spectral differences to drive the point layout. Figure 4c shows that the hierarchical embedding clearly separates the subcluster into two distinct groups. Projecting this subdivision back onto the image view reveals that the two groups correspond to the *heart chamber* and the *heart muscle*, two tissue types that are histologically distinct but spectrally similar enough to appear as a single cluster in the global embedding.

Step 4: Spectral validation. To validate the segmentation, Figure 4d compares the per-segment average spectra of the two subclusters against the average spectrum of the parent cluster from which they were derived – i.e., the single cluster containing the entire heart region prior to hierarchical refinement. The spectra of the two embedding-derived subclusters are clearly distinct, with the heart muscle exhibiting substantially higher absorbance in the glycogen band region when compared to the heart chamber. By contrast, the parent cluster spectrum is a blurred average of both signatures, reflecting the fact that the initial global embedding grouped these two chemically distinct tissue types together. This comparison demonstrates that the hierarchical embedding recovers chemically pure tissue signatures that the global embedding alone cannot resolve.

4.2. Use Case 2: Spectral Similarity Search and Spatial Overview

Dataset and goal. The second use case is based on two QCL-IR microscopy datasets of small areas of pigment samples deposited on an indium tin oxide-coated glass slide. Each dataset consists of 250 000 pixels across 843 channels. The analytical goal is to identify which of five known reference pigment spectra best matches the sample, supporting visual identification through spatial distribution and providing evidence for structural group membership based on spectral similarity patterns. The five reference pigments are Pigment Red 53:1 (PR53), Pigment Red 49 (PR49), Pigment Blue 15 (PB15), Pigment Orange 73 (PO73), and Pigment Red 122 (PR122). This workflow is representative of pigment authentication and verification tasks, where a measured sample must be matched against a library of known references.

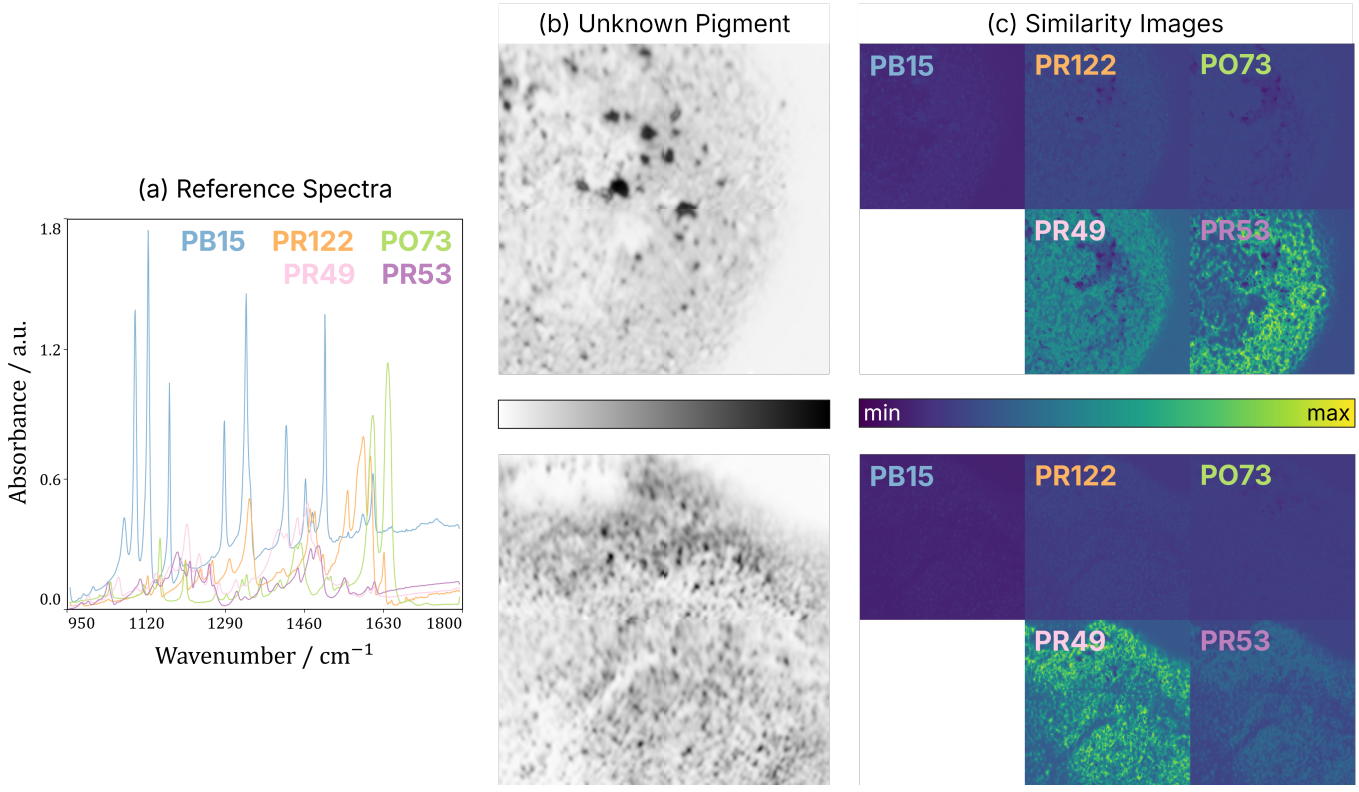

Fig. 5. Use Case 2: Spectral similarity search on two QCL-IR microscopy datasets of pigment samples (PR53 and PR49). (a) The five reference spectra representing known pigments, shown in the Spectrum Viewer. (b) Grayscale images of the two datasets showing the spatial distribution of the analyzed pigment on the slide. (c) Channel Glyph Viewer in linear mode, displaying the five similarity images for each dataset as glyphs: PR53 shows the highest similarity to the PR53 reference (top), and PR49 to the PR49 reference (bottom), while the structural similarity between the two pigments produces moderate cross-matches in both cases.

Computing similarity images. The five reference spectra are imported into the Spectrum Viewer. Before computing similarities, a baseline correction is applied to the dataset to reduce the influence of broad spectral offsets on the distance metric. Pixelwise similarities are then computed against each reference spectrum using a normalized Euclidean distance metric $s = 1/(1 + d)$, where d is the Euclidean distance between the pixel spectrum and the reference, yielding similarity scores $s \in (0, 1]$ with higher values indicating a closer match. For each reference spectrum, MIA produces one similarity image: a spatially resolved map in which intensity encodes the degree of spectral match at each pixel. The resulting similarity images are exported as a new dataset, effectively treating each reference spectrum as a channel in a derived dataset. Figure 5b shows the spatial distribution of the two pigment samples, confirming that the material is distributed across the slide in a spatially coherent pattern that can serve as a basis for similarity analysis.

Spatial overview via the Channel Glyph Viewer. With five similarity images per dataset, visual inspection of individual maps is straightforward, but comparing patterns across all references simultaneously benefits from an overview. The derived similarity datasets are loaded into the Channel Glyph Viewer in *linear* mode, where each channel – here, each similarity image – is displayed as a small spectral glyph arranged row by row. Figure 5c shows the result for both datasets: in each case, the highest similarity is observed for the matching reference pigment – PR53 for the first dataset and PR49 for the second – revealing the identity of the samples. Because PR53 and PR49 are structurally related pigments, moderate cross-similarity is also visible in both datasets, which is chemically expected and itself informative about the structural group membership of the sample. The Channel Glyph Viewer makes this pattern immediately apparent without requiring the analyst to inspect each similarity image individually.

Emergent use. This use case illustrates an emergent pattern not anticipated in the original design of the Channel Glyph Viewer, which was conceived primarily as a tool for exploring the full channel space of a hyperspectral dataset. In practice, users discovered that the linear layout serves equally well as a spatial overview of derived feature sets such as similarity images, repurposing a general-purpose view for a specific analytical task. This reflects a broader design principle of MIA: by keeping views general and linked through a shared data model, the tool accommodates analytical strategies that were not explicitly designed for.

4.3. Use Case 3: Multimodal Embedding

Dataset and goal. The third use case demonstrates MIA's multimodal analysis capabilities using a co-registered dataset combining QCL-IR microscopy and LA-ICP-MS measurements acquired on a parallel tissue section. The sample is a transverse thin section of human peripheral nerve tissue obtained from

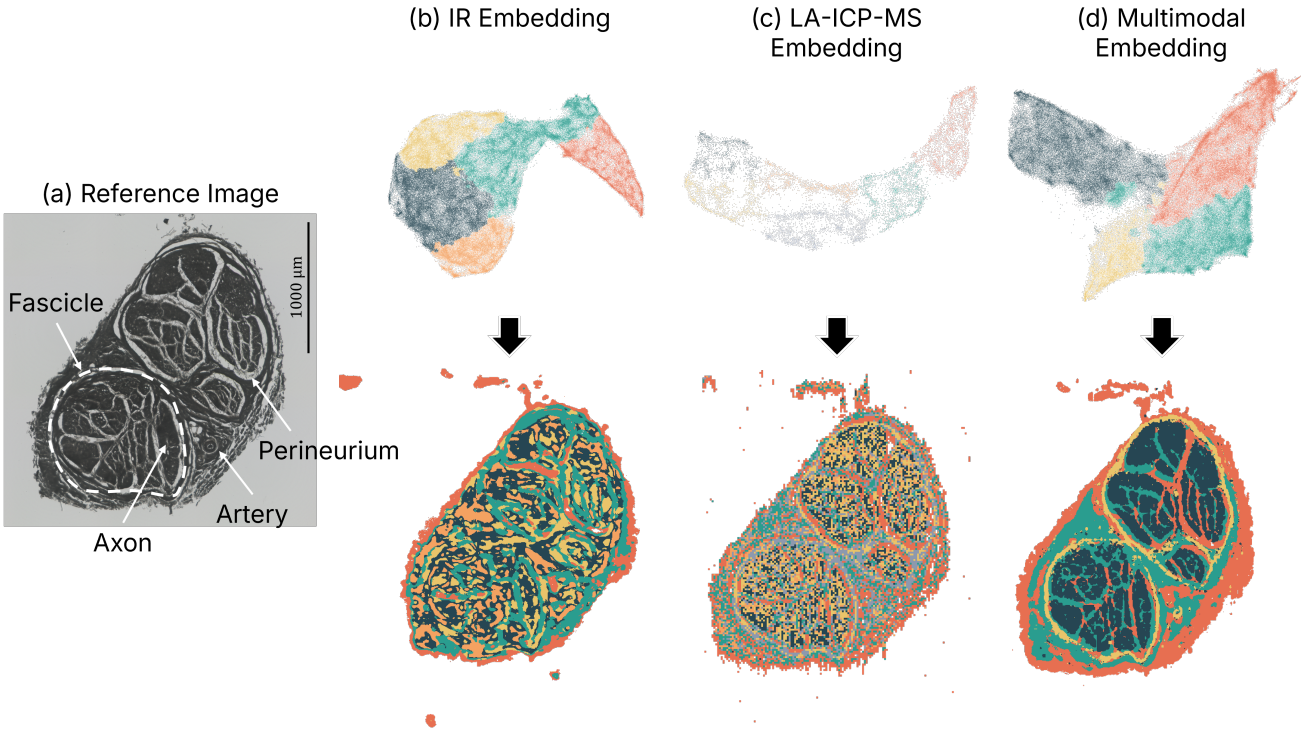

Fig. 6. Use Case 3: Multimodal embedding of co-registered QCL-IR microscopy and LA-ICP-MS data from a transverse section of human sciatic nerve tissue. (a) Brightfield reference image showing the anatomical structure of the section. (b) UMAP embedding and segmentation derived from IR data alone, resolving molecular tissue compartments. (c) UMAP embedding and segmentation derived from LA-ICP-MS data alone, reflecting elemental composition. (d) Combined multimodal embedding and segmentation: the integration of both modalities yields clearer compartment separation and supports the spatial investigation of gadolinium deposition within specific molecular tissue environments.

an autopsy. The scientific question motivating this dataset is whether gadolinium, a metallic element administered as a contrast agent during MRI examinations, is retained in the tissue after the procedure, and if so, in which tissue compartments it accumulates. This question requires both molecular tissue characterization (provided by IR microscopy across 211 spectral channels at 5 µm pixel size) and spatially resolved elemental composition (provided by LA-ICP-MS across 4 channels (Gd, Fe, Zn, P) at 15 µm pixel size), making it a natural candidate for multimodal analysis.

Individual embeddings. For the IR dataset, baseline correction and second-derivative preprocessing are applied before computing a UMAP embedding, followed by Leiden clustering. Figure 6b shows the resulting embedding and segmentation: the IR data resolves the major molecular tissue compartments of the peripheral nerve, including fascicles, perineurium, interfascicular connective tissue, and vascular structures, in good agreement with the brightfield reference image shown in Figure 6a. Figure 6c shows the analogous result for the LA-ICP-MS data alone, using the same embedding parameters applied to the four elemental channels: the elemental data captures a different aspect of tissue composition, reflecting the distribution of metals and phosphorus rather than molecular structure. While both individual embeddings produce anatomically interpretable segmentations, each reflects only one dimension of the tissue's chemical composition.

Multimodal embedding. The two datasets are loaded simultaneously into MIA, which resamples the LA-ICP-MS data to the IR spatial resolution (5 µm) using bilinear interpolation. A combined embedding is then computed using channels from both modalities. Because the IR dataset contains 211 channels compared to 4 elemental channels, the modality weighting dialog is used to balance their contributions to the embedding geometry; without weighting, the IR modality would dominate, and the elemental information would have negligible influence on the result. In this analysis, the modalities were weighted 1:2 (IR:LA-ICP-MS), giving the elemental information a stronger influence on the embedding. Figure 6d shows the resulting multimodal embedding and segmentation: the integration of both modalities yields clearer separation of anatomical compartments and more stable, consistent clusters than either modality alone. Crucially, the multimodal segmentation enables direct spatial correspondence between gadolinium-containing regions identified by LA-ICP-MS and the specific molecular tissue compartments characterized by IR, supporting the investigation of the biochemical environment in which gadolinium is deposited.

5. Discussion

5.1. Expert Feedback

MIA has been developed in close collaboration with researchers in analytical chemistry and has been used in published

research involving IR microscopy, micro-XRF, and LA-ICP-MS data [2, 38, 21]. To systematically gather feedback, we distributed a written questionnaire including the System Usability Scale (SUS) [39] to 6 domain experts. We note that the respondents are also collaborators on the development of MIA, which limits the independence of the evaluation. MIA received an average SUS score of 84.2 (SD = 8.76), corresponding to a rating of "good" on the Bangor et al. adjective scale [40]. The individual responses and the full questionnaire are provided in the supplementary material. The following summarizes the qualitative findings; we note that this constitutes expert feedback rather than a formal user study, which is consistent with the evaluation methodology of domain tool papers [41].

Collaborators consistently identified the combination of UMAP-based embedding and interactive segmentation as the most valuable part of MIA's workflow; all six respondents selected embedding as a frequently used feature, and five of six reported regular use of both manual and automatic segmentation. The ability to compute embeddings hierarchically within subclusters was specifically highlighted as enabling a level of analytical refinement that was not achievable with prior tools. As illustrated in Use Case 4.1, this iterative process revealed tissue-level distinctions that were invisible in the raw data and that the global embedding alone could not resolve. One respondent noted that "MIA has made my workflow more iterative and exploratory. I spend less time on manual preprocessing and switching between tools." Another observed that "segmentation based on dimensionality reduction helps to quickly identify substructures and patterns in the data."

The reduction in tool-switching was a recurring theme across respondents. When asked about their prior workflows, respondents reported using a mix of commercial vendor software, self-coded Python scripts, or ad-hoc combinations of individual analysis packages. MIA consolidates these steps into a single interface with a shared segmentation state, and respondents noted that this not only reduced time but also reduced the risk of inconsistencies introduced by transferring data between tools.

The emergent use of the Channel Glyph Viewer for spatial overview of similarity images (see Use Case 4.2) was not identified by us but discovered independently by collaborators during routine use. This finding reflects the value of providing flexible, general-purpose views that users can adapt to analytical needs beyond those explicitly anticipated in the design.

5.2. Limitations and Future Work

The following directions for future development were identified through collaborator feedback and reflect the boundaries of MIA's current scope.

Embedding alignment for consistent false-coloring. When comparing multiple embeddings of the same dataset – for example, embeddings computed with different parameters or applied to different modalities of a co-registered multimodal dataset – the false-coloring assigned to each embedding is independent, as the color mapping depends on the absolute positions of points in the 2D embedding space. This makes visual comparison across embeddings difficult, since corresponding pixels may receive entirely different colors in each view. A natural extension would be to align embeddings that share a point-to-point correspondence via a rigid transformation with uniform scaling, bringing their coordinate frames into a common reference and ensuring that corresponding pixels receive consistent colors across embeddings. This would be particularly valuable for the multimodal use case described in Section 4.3, where comparing per-modality and combined embeddings side by side is a central analytical step.

MALDI imaging with ion mobility spectrometry. Matrix-assisted laser desorption/ionization (MALDI) imaging with ion mobility separation produces data with a fundamentally different structure: each pixel is associated with a two-dimensional spectrum indexed jointly by mass-to-charge ratio (m/z) and reduced inverse ion mobility ($1/K_0$), rather than the one-dimensional spectrum along a single spectral axis assumed by MIA's data model. Supporting this modality would require extending the data model to accommodate 2D spectra per pixel, with corresponding changes to the Spectrum Viewer and feature computation. Given the growing importance of ion mobility spectrometry in molecular MSI, this represents a significant and worthwhile direction for future development.

Cohort analysis. MIA's multimodal framework currently requires datasets to be spatially co-registered, as the shared segmentation state is defined over a common set of pixels. This precludes a related but distinct analytical scenario: cohort analysis, in which multiple datasets from the same modality are acquired from different specimens or patients, and the analyst wishes to compute a combined embedding across the entire cohort without spatial alignment. Supporting cohort analysis would require a fundamentally different segmentation model and would open MIA to a broad class of comparative studies in biomedical imaging. We consider this the most consequential direction for future work.

6. Conclusion

We presented MIA, a modality-agnostic visual analysis environment for hyperspectral bioimaging that integrates spectral preprocessing, embedding-based dimensionality reduction, interactive segmentation, and spectral exploration within a single linked-view interface. By maintaining a shared segmentation state across all views and supporting a common data model for IR microscopy, LA-ICP-MS, and their multimodal combinations, MIA eliminates the tool-switching overhead that characterizes current analytical workflows in this domain.

Three use cases drawn from real collaborator workflows demonstrate the breadth of analytical scenarios MIA supports. The first showed that hierarchical UMAP embeddings applied to derivative-preprocessed IR spectra recover biologically meaningful tissue distinctions (heart chamber versus heart muscle) that are invisible in raw spectral data and unattainable through manual segmentation alone. The second demonstrated that spectral similarity analysis, combined with the Channel Glyph Viewer repurposed as a spatial overview tool, enables efficient identification of regions matching known reference compounds. The third illustrated how combining IR and LA-ICP-

MS data in a weighted multimodal embedding yields clearer separation of anatomical tissue compartments and enables direct localization of gadolinium deposits within specific molecular tissue environments – an insight not accessible from either modality individually. Together, these results demonstrate that integration and interactivity are independent contributions from algorithmic novelty in the development of analytical software for the biomedical and chemical imaging sciences. We hope that MIA lowers the barrier to sophisticated exploratory analysis for domain experts who are not computational specialists, and that its open design provides a foundation for future extensions to emerging modalities and study designs.

Acknowledgments

This work was supported in part by Deutsche Forschungsgemeinschaft (DFG) under Grant CRC 1450 – 431460824. The authors thank the Stiftung der Deutschen Wirtschaft gGmbH (sdw) for a scholarship to Hannes Gödde. The presented results have been achieved in the framework of the EFRE.NRW-funded project Pig-Pro-QuO (EFRE-20800668; IN-WP-2-005). We thank Astrid Jeibmann, Department of Radiology, University Hospital, Münster for her support. We thank Dr. Nassim Ghaffari-Tabrizi-Wizsy from the Otto Loewi Research Center, Division of Immunology, Medical University of Graz for her valuable support with the chicken embryo assay.

References

[1] Doble, PA, de Vega, RG, Bishop, DP, Hare, DJ, Clases, D. Laser ablation–inductively coupled plasma–mass spectrometry imaging in biology. Chemical reviews 2021;121(19):11769–11822.

[2] Kronenberg, K, Werner, J, Seeba, M, Rave, H, Linsen, L, Steiger, K, et al. A multimodal view at cancerous liver tissue by chemical bioimaging and image segmentation strategies. ChemRxiv 2023;2023(0925). doi:.

[3] Kröger, N, Egl, A, Engel, M, Gretz, N, Haase, K, Herpich, I, et al. Quantum cascade laser-based hyperspectral imaging of biological tissue. Journal of biomedical optics 2014;19(11):111607–111607.

[4] Schwaighofer, A, Brandstetter, M, Lendl, B. Quantum cascade lasers (QCLs) in biomedical spectroscopy. Chemical Society Reviews 2017;46(19):5903–5924.

[5] Walker, RA. Quantification of immunohistochemistry—issues concerning methods, utility and semiquantitative assessment i. Histopathology 2006;49(4):406–410. doi:.

[6] Toplak, M, Birarda, G, Read, S, Sandt, C, Rosendahl, SM, Vaccari, L, et al. Infrared Orange: Connecting hyperspectral data with machine learning. Synchrotron Radiation News 2017;30(4):40–45. doi:.

[7] Toplak, M, Read, ST, Sandt, C, Borondics, F. Quasar: Easy machine learning for biospectroscopy. Cells 2021;10(9). doi:.

[8] Bemis, KD, Harry, A, Eberlin, LS, Ferreira, C, van de Ven, SM, Mallick, P, et al. Cardinal: An R package for statistical analysis of mass spectrometry-based imaging experiments. Bioinformatics 2015;31(14):2418–2420. doi:.

[9] Bemis, KA, Föll, MC, Guo, D, Lakkimsetty, SS, Vitek, O. Cardinal v.3: A versatile open-source software for mass spectrometry imaging analysis. Nature Methods 2023;20(12):1883–1886. doi:.

[10] McInnes, L, Healy, J, Saul, N, Grossberger, L. UMAP: Uniform manifold approximation and projection. The Journal of Open Source Software 2018;3(29):861.

[11] Demšar, J, Curk, T, Erjavec, A, Gorup, Č, Hočevar, T, Milutinovič, M, et al. Orange: Data mining toolbox in python. the Journal of machine Learning research 2013;14(1):2349–2353.

[12] Jolliffe, I. Principal Component Analysis. John Wiley & Sons, Ltd. ISBN 9780470013199; 2005,doi:.

[13] Lasch, P. CytoSpec: Software for hyperspectral imaging. 2026. URL: https://www.cytospec.com/; Berlin, Germany. Accessed: March 26, 2026.

[14] Bruker Optics GmbH, . OPUS spectroscopy software. 2026. URL: https://www.bruker.com/; Ettlingen, Germany. Accessed: March 26, 2026.

[15] López-Fernández, H, de S. Pessôa, G, Arruda, MAZ, Capelo-Martínez, JL, Fdez-Riverola, F, Glez-Peña, D, et al. LA-iMageS: A software for elemental distribution bioimaging using LA–ICP-MS data. Journal of Cheminformatics 2016;8(1):65. doi:.

[16] Paton, C, Hellstrom, J, Paul, B, Woodhead, J, Hergt, J. Iolite: Freeware for the visualisation and processing of mass spectrometric data. J Anal At Spectrom 2011;26:2508–2518. doi:.

[17] Teledyne Photon Machines, . HDIP (hdf-based image processing) software. 2026. URL: https://www.teledynephotonmachines.com/support/hdip; Belgrade, USA. Accessed: March 26, 2026.

[18] Lockwood, TE, Westerhausen, MT, Doble, PA. Pew2: Open-source imaging software for laser ablation–inductively coupled plasma–mass spectrometry. Analytical Chemistry 2021;93(30):10418–10423. doi:; pMID: 34283564.

[19] Braun, G, Schaier, M, Werner, P, Theiner, S, Zanghellini, J, Wisgrill, L, et al. MeXpose–a modular imaging pipeline for the quantitative assessment of cellular metal bioaccumulation. JACS Au 2024;4(6):2197–2210. doi:.

[20] Andrews, HB, Hendriks, L, Irvine, SB, Dunlap, DR, Manard, BT. TOFHunter–unlocking rapid untargeted screening of inductively coupled plasma–time-of-flight–mass spectrometry data. J Anal At Spectrom 2025;40:910–920. doi:.

[21] Kronenberg, K, Rave, H, Ghaffari-Tabrizi-Wizsy, N, Nyckees, D, Elinkmann, M, Freitak, D, et al. Exploring high-dimensional LA-ICP-TOFMS data with uniform manifold approximation and projection (umap). J Anal At Spectrom 2025;40:3473–3484. doi:.

[22] Umfahrer, B, Buday, J, Pořízka, P, Kaiser, J, Garofalo, PS, Günther, D. Mineral phase-resolved quantification in la-icp-ms imaging. Analytical Chemistry 2026;98(1):581–589. doi:; pMID: 41406395.

[23] Cordes, J, Enzlein, T, Marsching, C, Hinze, M, Engelhardt, S, Hopf, C, et al. M2aia—interactive, fast, and memory-efficient analysis of 2d and 3d multi-modal mass spectrometry imaging data. GigaScience 2021;10(7):giab049. doi:.

[24] van der Maaten, L, Hinton, GE. Visualizing data using t-SNE. Journal of Machine Learning Research 2008;9(86):2579–2605. URL: http://jmlr.org/papers/v9/vandermaaten08a.html.

[25] Cashman, D, Keller, M, Jeon, H, Kwon, BC, Wang, Q. A critical analysis of the usage of dimensionality reduction in four domains. IEEE Transactions on Visualization and Computer Graphics 2025;31(10):9405–9423. doi:.

[26] Pezzotti, N, Höllt, T, Lelieveldt, B, Eisemann, E, Vilanova, A. Hierarchical stochastic neighbor embedding. Computer Graphics Forum 2016;35(3):21–30. doi:.

[27] van Unen, V, Höllt, T, Pezzotti, N, Li, N, Reinders, M, Eisemann, E, et al. Visual analysis of mass cytometry data by hierarchical stochastic neighbour embedding reveals rare cell types. Nature Communications 2017;8(1). doi:.

[28] Traag, VA, Waltman, L, van Eck, NJ. From Louvain to Leiden: Guaranteeing well-connected communities. Scientific Reports 2019;9(1):5233. doi:.

[29] Wolf, FA, Hamey, FK, Plass, M, Solana, J, Dahlin, JS, Göttgens, B, et al. PAGA: graph abstraction reconciles clustering with trajectory inference through a topology preserving map of single cells. Genome Biology 2019;20(1):59. doi:.

[30] McInnes, L, Healy, J, Astels, S, et al. hdbscan: Hierarchical density based clustering. J Open Source Softw 2017;2(11):205.

[31] Jordan, J, Angelopoulou, E, Maier, A. A novel framework for interactive visualization and analysis of hyperspectral image data. Journal of Electrical and Computer Engineering 2016;2016(1):2635124. doi:.

[32] Jawad, M, Soltwisch, J, Dreisewerd, K, Linsen, L. Interactive visual analysis of mass spectrometry imaging data using linear and non-linear embeddings. Information 2020;11(12). doi:.

[33] Zhu, F, Pan, Y, Gao, T, Walia, H, Yu, H. Interactive visualization of hyperspectral images based on neural networks. IEEE Computer Graphics and Applications 2021;41(5):57–66. doi:.

[34] Yu, H, Li, S. Feature selection-oriented interactive visual anal-

ysis approach for hyperspectral images. Information Visualization 2025;24(3):284–297. doi:.

[35] Mörth, E, Sidak, K, Maliga, Z, Möller, T, Gehlenborg, N, Sorger, P, et al. Cell2Cell: Explorative cell interaction analysis in multi-volumetric tissue data. IEEE Transactions on Visualization and Computer Graphics 2025;31(1):569–579. doi:.

[36] Rave, H, Molchanov, V, Linsen, L. De-cluttering scatterplots with integral images. IEEE Transactions on Visualization and Computer Graphics 2025;31(4):2114–2126. doi:.

[37] Ramshaw, L, Tarjan, RE. On minimum-cost assignments in unbalanced bipartite graphs. HP Labs, Palo Alto, CA, USA, Tech Rep HPL-2012-40R1 2012;20:14.

[38] Peivandi, AD, Holtkamp, M, Rave, H, Linsen, L, Martens, S, Müller, KM, et al. Rapid versus slow degeneration and complications of biomaterials in patients with congenital heart disease. Cardiovascular Pathology 2025;75:107712. doi:.

[39] Brooke, J, et al. SUS—a quick and dirty usability scale. Usability Evaluation in Industry 1996;189(194):4–7.

[40] Bangor, A, Kortum, P, Miller, J. Determining what individual SUS scores mean: Adding an adjective rating scale. Journal of Usability Studies 2009;4(3):114–123.

[41] Sedlmair, M, Meyer, M, Munzner, T. Design study methodology: Reflections from the trenches and the stacks. IEEE Transactions on Visualization and Computer Graphics 2012;18(12):2431–2440. doi:.